Plasma Sources Science and Technology

PAPER

Spatial thermal dose delivery in atmospheric pressure plasma jets

To cite this article: Dogan Gidon *et al* 2019 *Plasma Sources Sci. Technol.* **28** 025006

IOP Publishing Plasma Sources Science and Technology
Plasma Sources Sci. Technol. **28** (2019) 025006 (11pp) https://doi.org/10.1088/1361-6595/aafff6

Spatial thermal dose delivery in atmospheric pressure plasma jets

Dogan Gidon, David B Graves and Ali Mesbah

Department of Chemical and Biomolecular Engineering, University of California, Berkeley, CA 94720, United States of America

E-mail: graves@berkeley.edu and mesbah@berkeley.edu

Received 12 September 2018, revised 13 December 2018
Accepted for publication 18 January 2019
Published 25 February 2019

Abstract

Atmospheric pressure plasma jets (APPJs) are increasingly used in plasma medicine and materials processing applications. Reproducible and effective operation of APPJs requires regulating the cumulative effects of plasma on a target substrate in the face of variabilities and exogenous disturbances. This article investigates spatial delivery of thermal effects—thermal dose—of plasma using a kHz-excited APPJ in helium translated over a dielectric substrate. A dose metric is presented for quantifying the cumulative, nonlinear thermal effects of plasma along the translation trajectory of the APPJ. An optimization-based feedback control strategy is proposed for real-time regulation of thermal dose delivery using spatial measurements of substrate temperature. Experimental investigation reveals that feedback control is crucial for achieving spatially uniform dose delivery.

Keywords: atmospheric pressure plasma jets, dose delivery, feedback control

1. Introduction

Plasma medicine hinges on local generation and delivery of a variety of therapeutic agents including electric fields, reactive chemical species, and thermal effects. With an increasing number of clinically approved atmospheric pressure plasma devices such as KINPen (neoplas tools GmbH, Greifswald, Germany) [1] and SteriPlas (Adtec Plasma Technology, Adtec Europe, Hunslow, UK) [2], there is growing evidence for the effectiveness of plasma medicine in alternative and complementary therapies such as reduction of head and neck cancer [3] and accelerated healing of chronic wounds [4]. In the absence of reliable dosimetry and online diagnostics, however, the common practice in plasma medicine is to devise treatment protocols offline, largely based on user's experience and device characteristics. The primary challenges in this approach arise from quantifying the complex interactions between plasma and target substrate as well as achieving uniform delivery of therapeutically effective *plasma dose* across a substrate in the face of inherent variabilities of plasma dynamics, exogenous disturbances, and uneven substrate characteristics.

Generally, accurate quantification of therapeutic doses is challenging due to lack of direct measurements for short- and long-term biological effects of a therapy [5]. This challenge is further aggravated in plasma medicine because of the presence of multitude of different therapeutic effects (i.e. thermal, chemical, and electrical) and their synergistic interactions [6, 7]. Although dose quantification is highly specialized in different therapies, dose metrics share some commonalities: (i) they should describe the cumulative, *non-retractable* nature of a therapeutic effect, and (ii) they should be defined in terms of a measurable property of a target substrate, which is related to some characteristics of underlying biological processes (e.g. volumetric energy absorbed as ionizing radiation in radiotherapy [5], or substrate temperature in hyperthermia [8]). Additionally, concepts such as *isodose* in radiotherapy [5] or *equivalent dose* in hyperthermia [9] are commonly adopted in order to quantify how therapeutic effects vary under different treatment protocols relative to a reference treatment condition or protocol.

This article investigates *thermal dose* delivery in atmospheric pressure plasma jets (APPJs), which are increasingly used in plasma medicine [10]. APPJs consist of a noble gas (typically He or Ar) that flows through a dielectric tube at a rate of $\sim$1–10 slm. The small dimensions (few mm in diameter), cheap construction, and low power consumptions ($\leqslant$10 W) make APPJs suitable for use as portable and handheld therapeutic tools [11]. APPJs also provide versatility in enhancing the plasma chemistry and thus its therapeutic

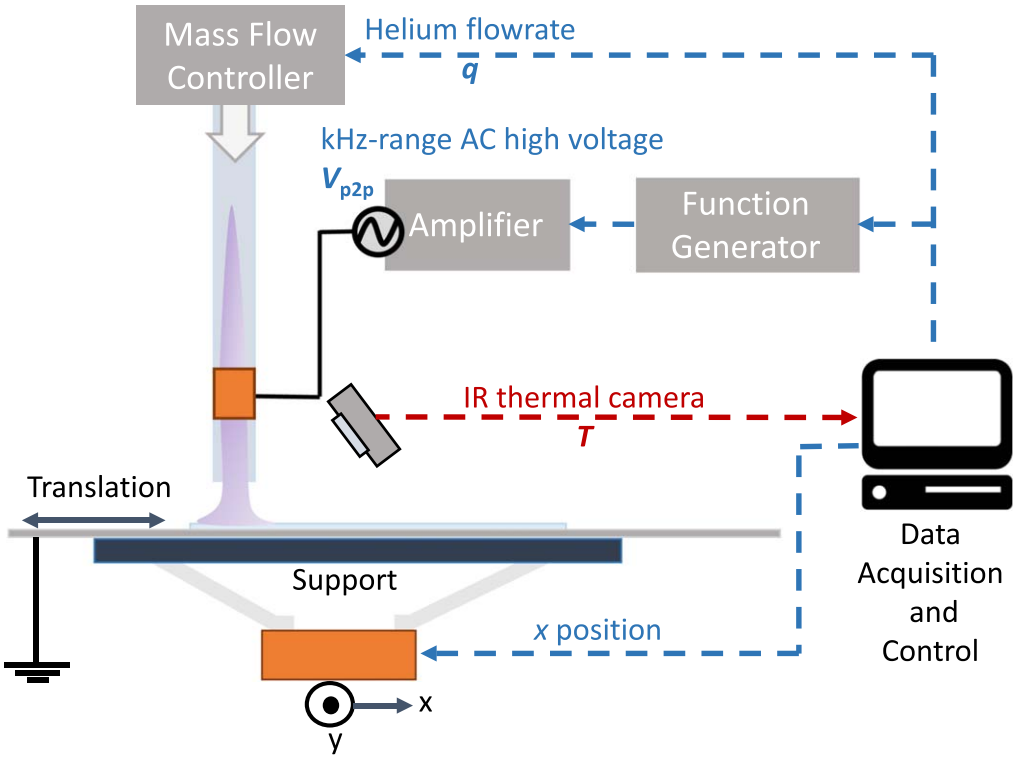

Figure 1. Schematic of the kHz-excited APPJ in helium. Signals are shown in dashed lines, with measurement signals indicated in red and actuation signals indicated in blue.

effects by using admixutres of small amounts of molecular gases such as nitrogen, oxygen, or water vapor [12]. However, the inherent nonlinearities [13, 14], long timescale drifts [15], and run-to-run variations [16], as well as sharp gradients of species concentrations, gas temperature, and electric fields axially along the flow axis [17] and radially on the substrate [18], pose unique challenges to reproducible and therapeutically effective operation of APPJs. Furthermore, APPJs exhibit high sensitivity to external factors—exogenous disturbances—such as the separation distance between the APPJ tip and target substrate [19, 20], concentration of ambient species [21], and uneven properties (e.g. electrical or thermal) of the substrate [18]. Additionally, small dimensions of APPJs often necessitate their translation over a substrate in order to fully treat the target area. The APPJ translation introduces further variabilities in plasma characteristics that can compromise reproducible and effective operation of APPJs.

We have recently demonstrated the usefulness of model-based feedback control for mitigating the effects of variabilities and disturbances on APPJ operation [20, 22, 23]. In this article, we address the problem of uniform delivery of thermal dose of a kHz-excited APPJ in helium along its translation trajectory. Drawing from thermal dosimetry in hyperthermia [8], we first present a dose metric for quantifying the cumulative, nonlinear thermal effects of the APPJ using spatial measurements of substrate temperature. An optimization-based feedback control strategy is then proposed for real-time regulation of thermal dose delivery as the APPJ is translated over a dielectric substrate. The performance of the feedback control strategy is demonstrated under different APPJ translation trajectories, where experimental investigations indicate the critical role of real-time regulation of dose delivery and feedback control for achieving spatially uniform dose delivery.

2. Experimental setup

A schematic of the kHz-excited APPJ in helium is shown in figure 1. The plasma is generated in a dielectric, quartz tube (ID = 3 mm and OD = 4 mm) by applying sinusoidal voltage at a frequency of 20 kHz to a copper ring electrode. A borosilicate microscope cover slip (LSS, 24 × 50 × 0.15 mm) placed over a grounded aluminum plate is used as the substrate. The separation distance between the substrate and the tube nozzle is maintained at 4 mm. The setup is equipped with a x–y movement table controlled by stepper motors that translate the substrate.

The actuation of the APPJ setup consists of the He flow rate $q \in [0, 4\ \text{slm}]$, the applied peak-to-peak voltage $V_{p2p} \in [6, 10\ \text{kv}]$, and the substrate position $x \in [-10, 10\ \text{mm}]$, which are implemented using micro controllers (Arduino UNO R3). The He flow rate is set at 1.5 slm, whereas the applied peak-to-peak voltage is manipulated to control the substrate temperature (see section 4). Temperature of the substrate, T, is measured every 1.3 s using a radiometric infrared (IR) thermal camera (Lepton FLIR). The substrate temperature is readily extracted from the thermal images; see figure 2 for a

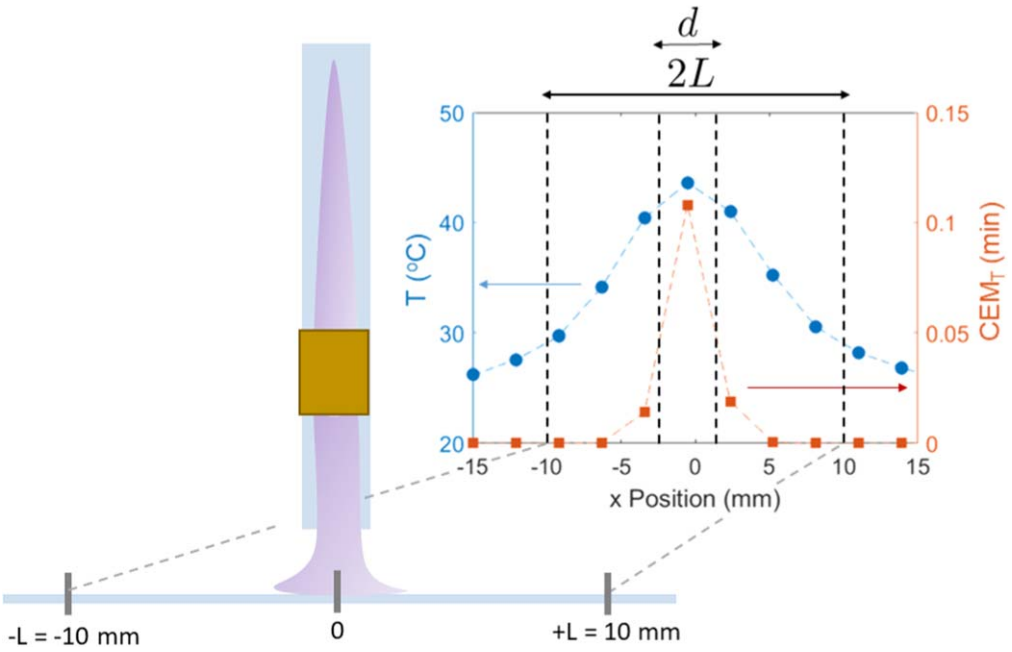

Figure 2. A representative measurement of the substrate temperature obtained from the IR thermal images and its corresponding thermal dose $\mathrm{CEM_T}$ delivered over 1.3 s along the translation trajectory $x \in [-L, L]$. d denotes the tube diameter of the APPJ.

representative measurement. Open-source hardware is used to implement the data acquisition and control system. A single board computer (Raspberry Pi 3) is used for data logging and coordination. Control algorithms are implemented on a WiFi-enabled laptop that communicates with the single board computer using the TCP/IP protocol.

To mitigate the variabilities associated with start-up of the APPJ, we allow a 20 min warm-up period between the plasma ignition and the start of an experiment in all APPJ runs. Between each run, the applied peak-to-peak voltage is kept at its minimum (i.e. $\mathrm{V_{p2p}} = 6$ kV) for a period of 5 min to ensure that the substrate temperature dynamics have settled. All experiments are conducted in triplicates.

3. Thermal dose delivery

Treatment protocols in plasma medicine are commonly designed based on user's experience in terms of some reference operating parameters of a hand-held plasma device, treatment time, and *translation rate* of the plasma device on a target substrate [3]. Ideally, however, the objective of plasma treatment is to deliver a predetermined plasma dose to a target substrate within a prespecified treatment time frame as the plasma device is translated over the substrate. This suggests that effective plasma dose delivery hinges on: (i) quantifying the cumulative effects of plasma on the target substrate in terms of tempo-spatial variations of substrate properties that are intimately related to the plasma effects and (ii) systematic translation of the plasma device over the substrate. Here, we demonstrate the notion of spatial dose delivery for the thermal effects of the APPJ in figure 1 when the APPJ is translated along the x-direction.

3.1. Spatial metric for thermal dose

Controlling the thermal effects of plasma in medical therapies is important for patient safety and comfort [24]. Thermal dosimetry is fairly well-established in hyperthermia treatment, where the thermal dose is commonly quantified point-wise using the *Cumulative Equivalent Minutes* ($\mathrm{CEM_T}$) metric that is defined at a reference treatment temperature of 43 °C [8, 25, 26]. At any target point x, $\mathrm{CEM_T}$ is expressed as

$$\mathrm{CEM_T}(\tau, x) = \int_0^{\tau} K^{(43 - T(t,x))}\, \mathrm{d}t, \tag{1}$$

where τ is a prespecified treatment time and the constant K characterizes the substrate response to thermal stresses

$$K = \begin{cases} 0 & T(t, x) \leqslant 39^{\circ}\mathrm{C} \\ 0.25 & 39^{\circ}\mathrm{C} < T(t, x) < 43^{\circ}\mathrm{C} \\ 0.5 & T(t, x) \geqslant 43^{\circ}\mathrm{C}. \end{cases}$$

The thermal dose metric $\mathrm{CEM_T}$ has a unit of time. The constant K implies that the rate of thermal dose accumulation doubles for every 1 °C increase in the substrate temperature above the reference temperature 43 °C, whereas the accumulation rate halves when the substrate temperature is in the range of 39 °C – 43 °C. Thus, expression (1) suggests that the thermal effects on a substrate are nonlinear and non-decreasing, that is, the delivered thermal dose cannot be retracted. Note that there is no thermal dose accumulation below 39 °C.

We adopt the above $\mathrm{CEM_T}$ metric for quantifying the tempo-spatial thermal effects of the APPJ along the translation trajectory x (see figure 1). Based on empirical observations of substrate temperature shown in figure 2, a Gaussian parameterization can be used to describe the spatial

Table 1. Four cases for the translation rate of the APPJ, which are specified in terms of characteristic time Δt and length Δx.

	Δx (mm)	Δt (s)
Case I	7	100
Case II	2	30
Case III	1	7.8
Case IV	0.5	1.3

distribution of substrate temperature along x

$$T(t, x) = (T_{\max}(t) - T_{\inf})\mathrm{e}^{-\frac{(x-\mu(t))^2}{\sigma^2(t)}} + T_{\inf}. \quad (2)$$

Expression (2) suggests that substrate temperature at any point along the translation trajectory $x \in [-L, L]$ can be described in terms of: (i) the maximum substrate temperature $T_{\max}(t)$ at the centerline of the APPJ, which determines the highest rate of dose accumulation according to the $\mathrm{CEM_T}$ metric in (2), (ii) the spatial variance of substrate temperature around the APPJ centerline $\sigma^2(t)$, and (iii) the position of the APPJ centerline $\mu(t)$, which is governed by the APPJ translation rate. $T_{\inf}$ denotes the ambient temperature in (2) and is used to normalize the temperature distribution. As discussed in section 4, the parameters $T_{\max}(t)$, $\sigma^2(t)$, and $\mu(t)$ can in principle be controlled for regulation of the thermal dose delivery along x.

3.2. Translation rate

To treat areas larger than the dimensions of the APPJ, it is necessary to translate the APPJ over the target substrate. The common practice in plasma medicine is to translate the APPJ in a 'meandering pattern' to achieve an average treatment rate of approximately 1 $\mathrm{cm^2\,min^{-1}}$ [3, 27]. Generally, prespecifying the APPJ translation rate systematically to achieve a desired spatial dose profile across the treatment area is not trivial. In radiotherapy, the device translation is typically specified in terms of either discrete translation steps (i.e. *step-and-shoot* strategy), or continuous translation with some velocity (i.e. *moving window* strategy) [28]. Inspired by the step-and-shoot strategy, a discrete translation scheme is adopted for the APPJ in figure 1. The APPJ translation rate is defined in terms of discrete steps of size Δx, where the APPJ is held for a time interval of Δt at each step. Δx and Δt can be chosen based on the characteristic time and length scales of the APPJ dynamics. Under nominal APPJ operation ($V_{\mathrm{p2p}} = 8$ kV and $q = 1.5$ slm), the characteristic time of the substrate temperature dynamics is 30 s, whereas the spatial distribution of substrate temperature has a variance of approximately 7 $\mathrm{mm^2}$ (i.e. $\sigma^2 = 7\,\mathrm{mm^2}$ in (2)). However, due to the exponential nature of the dose metric (1), $\sigma^2(t)$ is considerably larger than the region over which dose accumulates (see figure 2). The characteristic length of the thermal dose accumulation is observed to be similar to the radius of the substrate area across which the plasma spreads.

Table 1 lists the time- and length-scale characteristics of four cases for the translation rate of the APPJ, as considered in the remainder of this article. Note that Cases I and IV correspond to two extreme translation rates: a discrete translation with few long steps in Case I and a 'continuous' translation with many short steps in Case IV.

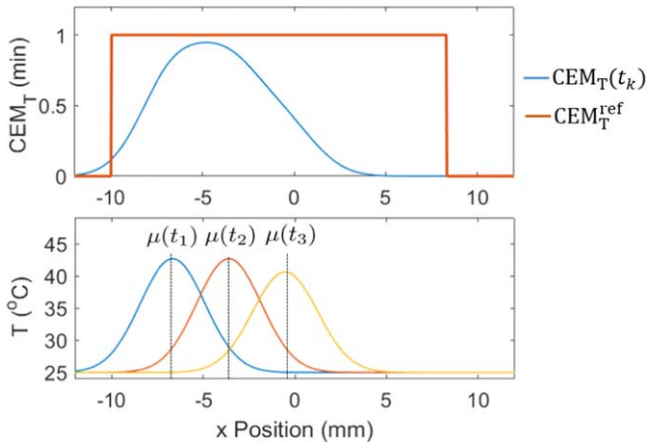

Figure 3. Depiction of thermal dose delivery along the APPJ translation trajectory $x \in [-L, L]$ at an arbitrary time point t_k. The accumulated thermal dose $\mathrm{CEM_T}$ (top) is quantified in terms of spatial measurements of the substrate temperature obtained in real time along the translation trajectory x (bottom). μ denotes the centerline of the APPJ, which shifts along the translation trajectory.

4. Real-time regulation of thermal dose delivery

We aim to investigate uniform delivery of thermal dose $\mathrm{CEM_T}(\tau, x)$ along the APPJ translation trajectory $x \in [-L, L]$ under the APPJ translation rates listed in table 1. A schematic of spatially uniform thermal dose delivery is given in figure 3. To achieve uniform thermal dose delivery, we propose the hierarchical, feedback control strategy shown in figure 4 to control the spatial distribution of substrate temperature along the translation trajectory. At the lower-level of the control strategy, a proportional-integral (PI) controller is used to control the maximum substrate temperature $T_{\max}$ at the centerline of the APPJ via manipulating the applied peak-to-peak voltage V_{p2p}. The PI controller is given by

$$V_{\mathrm{p2p}}(t) = k_p\Big((T^{\mathrm{ref}}_{\max}(t) - T_{\max}(t)) + \frac{1}{\tau_i}\int_0^t (T^{\mathrm{ref}}_{\max}(t') - T_{\max}(t'))dt'\Big), \quad (3)$$

where $T^{\mathrm{ref}}_{\max}$ is the *reference* maximum substrate temperature and k_p and τ_i are tuning parameters determined using IMC rules [29] (see appendix). The PI controller computes the control input V_{p2p} every 1.3 s as $T_{\max}$ is measured. Physical bounds of the control input V_{p2p} are incorporated into the PI controller via addition of anti-windup effect [30].

The PI controller enables tracking the reference temperature $T^{\mathrm{ref}}_{\max}$ in the presence of exogenous disturbances acting on the APPJ. However, the PI controller cannot account for the cumulative, nonlinear nature of the thermal dose $\mathrm{CEM_T}(\tau, x)$. Thus, we propose an optimization-based supervisory controller for determining the reference

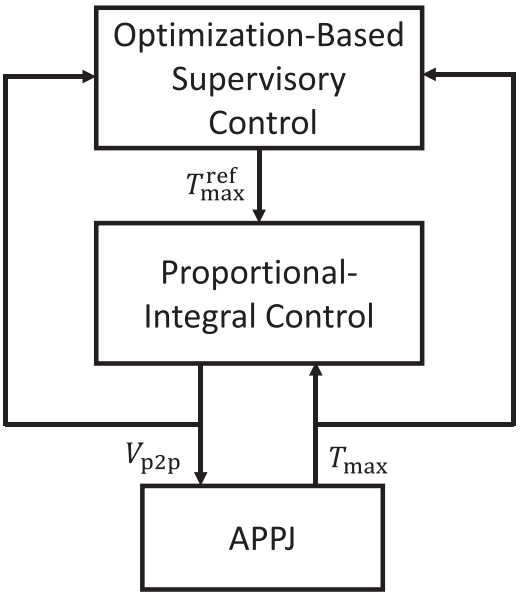

Figure 4. The hierarchical, feedback control strategy for real-time regulation of thermal dose delivery using the APPJ. The control strategy consists of: (i) a proportional-integral (PI) controller that regulates the maximum substrate temperature $T_{\max}$ at the APPJ centerline via manipulating the applied peak-to-peak voltage V_{p2p} every 1.3 s, and (ii) an optimization-based supervisory controller that plans the thermal dose delivery every 6 s via determining the optimal values for the reference maximum substrate temperature $T_{\max}^{\mathrm{ref}}$ in the PI controller based on the user-specified treatment time, the reference thermal dose along the translation trajectory, and the APPJ translation rate.

temperature $T_{\max}^{\mathrm{ref}}$ (see figure 4). Given the accumulated thermal dose $\mathrm{CEM_T}(t_k, x)$ up to sampling time t_k over $x \in [-L, L]$, the supervisory controller solves the dynamic optimization problem

$$\min_{T_{\max}^{\mathrm{ref}}(t)} \int_{-L}^{L} \|\mathrm{CEM_T}(\tau, x)\mathrm{d}x - \mathrm{CEM_T^{ref}}(\tau, x)\|^2 + \int_{t_k}^{\tau} \|\mathrm{d}T_{\max}^{\mathrm{ref}}(t)\|_w^2 \mathrm{d}t \tag{4a}$$

$$\text{s.t. } \frac{\mathrm{dCEM_T}(t, x)}{\mathrm{d}t} = K^{(43 - T(t,x))}, \tag{4b}$$

$$T(t, x) = (T_{\max}^{\mathrm{ref}}(t) - T_{\mathrm{inf}})\mathrm{e}^{-\frac{(x-\mu(t))^2}{\sigma^2(t)}} + T_{\mathrm{inf}}, \tag{4c}$$

$$T_{\max}^{\mathrm{ref}}(t) \leqslant 45°\mathrm{C}, \quad t \in [t_k, \tau], \quad x \in [-L, L], \tag{4d}$$

where $T_{\max}^{\mathrm{ref}}(t)$ over the time horizon $[t_k, \tau]$ is the decision variable of the optimization problem, τ is the user-specified treatment time in the thermal dose metric (1), $\mathrm{CEM_T^{ref}}(\tau, x)$ is the user-specified *reference* thermal dose at the end of the treatment time τ along the translation trajectory $x \in [-L, L]$, and w is a user-specified constant weight. In the optimization (4), the first term of the objective function (4*a*) describes the integral of squared deviations between the predicted and reference thermal dose at τ. The second term in (4*a*) penalizes excessive changes in the decision variable $T_{\max}^{\mathrm{ref}}(t)$ to avoid abrupt changes in the substrate temperature. Expressions (4*b*) and (4*c*) describe the time evolution of thermal dose accumulation in terms of the dose metric (1) and the Gaussian parameterization of distribution of substrate temperature along x (see expression (2)). The thermal dose accumulation predicted by (4*b*) is dependent on the initial thermal dose $\mathrm{CEM_T}(t_k, x)$ and the translation rate of the APPJ centerline $\mu(t)$. The constraint (4*d*) ensures that the maximum substrate temperature remains below some user-specified threshold, for example, to ensure patient safety and comfort.

The dynamic optimization problem (4) is solved repeatedly in real time every 6 s to enable *closed-loop* thermal dose delivery planning . This entails re-initializing (4) at every sampling time t_k based on the thermal dose $\mathrm{CEM_T}(t_k, x)$ accumulated up to time t_k (i.e. inferred from the substrate temperature measurements), solving the optimization, and subsequently applying the optimal value for $T_{\max}^{\mathrm{ref}}(t_k)$ to the lower-level PI controller as its reference. The repeated solution of the optimization confers a measurement feedback action to the thermal dose delivery planning in order to provide some degree of robustness to unmeasured disturbances affecting the dose delivery. Alternatively, the optimization (4) can be solved offline—only once, before the treatment—to determine an optimal trajectory for $T_{\max}^{\mathrm{ref}}(t)$ over the treatment time $[0, \tau]$. We refer to this strategy as *open-loop* thermal dose delivery planning. In this work, the optimization (4) is solved using automatic differentiation software CasADi [31] and the interior point optimization library IPOPT [32] in Python.

It follows from above that the PI controller enables fast rejection of disturbances acting on the APPJ, whereas the optimization-based supervisory controller allows for planning the thermal dose delivery in terms of the treatment time τ, the reference thermal dose $\mathrm{CEM_T^{ref}}(\tau, x)$ along the translation trajectory $x \in [-L, L]$, and the APPJ translation rate as specified in table 1. We remark that other parameters characterizing the spatial distribution of substrate temperature in expression (2)—namely the spatial variance of substrate temperature around the APPJ centerline, σ^2, and the APPJ position, μ—can be considered in the optimization (4) as decision variables. To the extent that σ^2 can be measured and manipulated effectively, the distribution of the substrate temperature can be controlled to realize a desired spatial distribution of the reference thermal dose $\mathrm{CEM_T^{ref}}(\tau, x)$. Optimizing for μ in the optimization (4), on the other hand, can allow for determining an optimal translation trajectory. Although these alternative formulations for the optimization (4) can introduce further computational and/or implementation complexities (e.g. increased solution time of optimization, or a multivariable lower-level control structure), the hierarchical, optimization-based control strategy in figure 4 provides a versatile framework for real-time regulation of spatial dose delivery.

5. Results and discussion

The proposed feedback control strategy is implemented on the APPJ shown in figure 1, where the objective is to deliver a thermal dose of 1 min uniformly over a translation distance of 20 mm during treatment time of $\tau = 5$ min. Thus, the

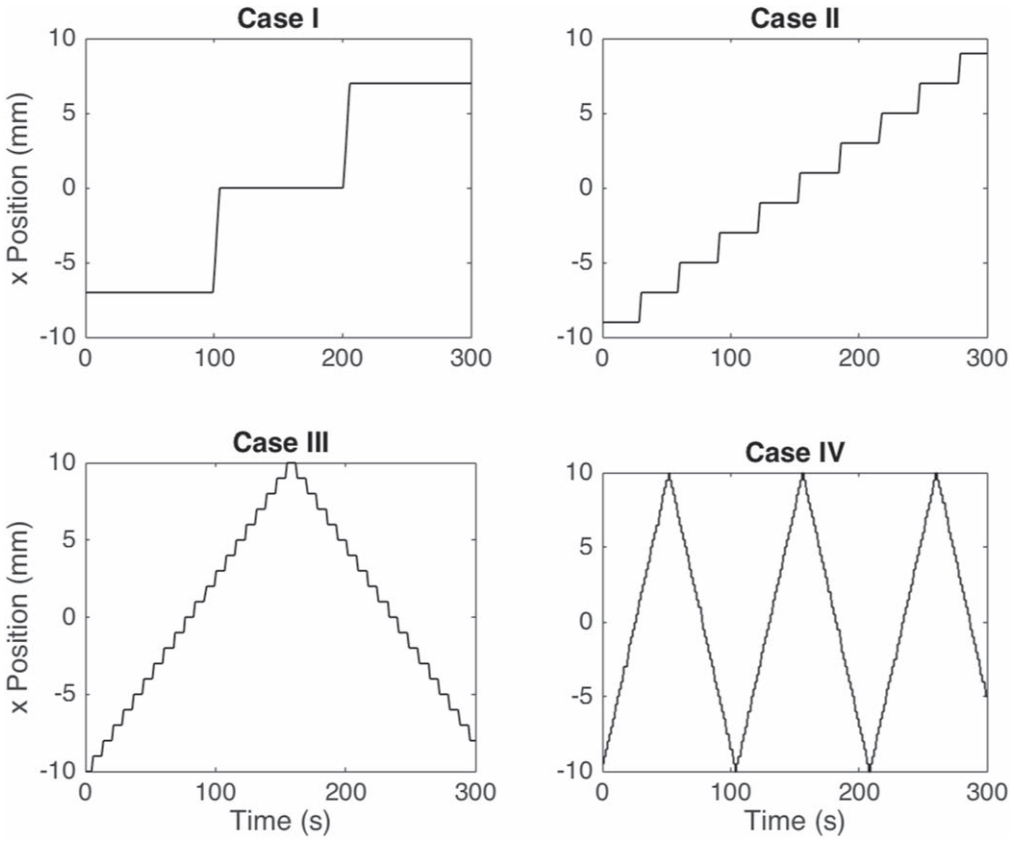

Figure 5. The translation trajectories of the APPJ under the four translation rates given in table 1. The translation rate increases from Case I to Case IV while the target region and treatment time remain fixed at 20 mm and 5 min, respectively.

reference thermal dose in the optimization problem (4) is defined as

$$\mathrm{CEM}_{\mathrm{T}}^{\mathrm{ref}}(5, x) = \begin{cases} 1 & -10\ \mathrm{mm} \leqslant x \leqslant 10\ \mathrm{mm} \\ 0 & \text{otherwise.} \end{cases} \tag{5}$$

Figure 5 shows the APPJ translation trajectories corresponding to the four APPJ translation rates given in table 1. We remark that the translation direction of the APPJ is reversed during the treatment in Cases III and IV. This is because the APPJ translation rate in these two cases is high—relative to that in Cases I and II—for the target region be treated in a 'single pass' given the fixed treatment time of 5 min.

In the reminder of this section, we first demonstrate the usefulness of the PI controller for mitigating the effect of exogenous disturbances and variabilities on the APPJ operation. We then investigate the performance of the hierarchical, optimization-based control strategy for real-time regulation of thermal dose delivery under the APPJ translation trajectories depicted in figure 5.

5.1. Why feedback control?

The substrate temperature is affected by the intrinsic variabilities of plasma and exogenous disturbances acting on the APPJ (e.g. ambient temperature and humidity). Here, we demonstrate the capability of the PI controller in mitigating these effects under the translation trajectory of Case I shown in figure 5. Figure 6 shows the maximum substrate temperature, $T_{\max}$, profiles for the cases of (a) no feedback control (i.e. constant applied peak-to-peak voltage V_{p2p}), and (b) PI control. For each case, two sets of experiments are carried out on different days under different ambient temperature, where each run is replicated three times.

In the case of no feedback control, figure 6(a) suggests that $T_{\max}$ is sensitive to ambient temperature and there is considerable variability over the three replicate runs. The effect of the APPJ translation is also reflected in the $T_{\max}$ profile, where abrupt changes at $t = 100$ s and $t = 200$ s are observed—consistent with the APPJ translation shown in figure 5. Under the translation trajectory of Case I, the timescale of APPJ translation is on par with that of the substrate temperature dynamics. Thus, when the APPJ is translated to a new point (e.g. at $t = 100$ s), that point has already been exposed to thermal energy due to spatial distribution of substrate temperature along the target region x. This presents one possible explanation for the observed increase in $T_{\max}$ as the APPJ is translated over the target region. Since the discharge is highly sensitive to external conditions, other disturbances such as inhomogeneity in substrate properties or small changes in separation distance along the movement direction can also affect the thermal behavior. Clearly, the substrate temperature behavior in the case of no feedback control is undesirable, especially when treating a heat-sensitive substrate. This motivates the need for a feedback control strategy that can regulate substrate temperature in the presence of variabilities and disturbances.

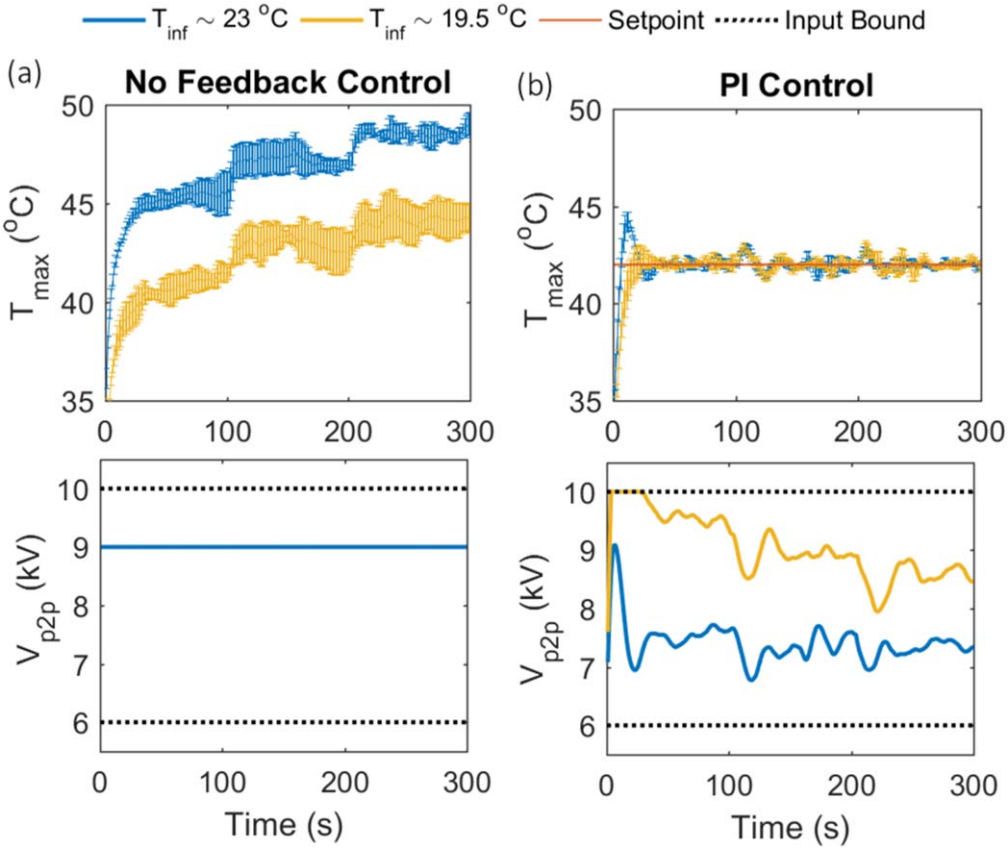

Figure 6. Maximum substrate temperature $T_{\max}$ and applied peak-to-peak voltage V_{p2p} under the APPJ translation rate of Case I in table 1 for the cases of: (a) no feedback control and (b) PI control with the reference maximum substrate temperature $T_{\max}^{\mathrm{ref}} = 42^{\circ}$ C. Two sets of experiments are carried out for each case under different ambient temperature T_{inf}. The error bars show the standard deviation of temperature measurements based on three replicate runs.

On the other hand, figure 6(b) suggests that the PI controller can effectively maintain $T_{\max}$ at its arbitrarily chosen reference $T_{\max}^{\mathrm{ref}} = 42^{\circ}$ C. The PI controller is able to maintain the user-specified reference temperature under both ambient temperatures, while significantly reducing the variability of $T_{\max}$ across the replicate runs. This is achieved by manipulating the applied peak-to-peak voltage V_{p2p} based on real-time substrate temperature measurements. In order to maintain $T_{\max}$ constant, the input V_{p2p} varies considerably during the operation. We note that, although this is acceptable from the standpoint of controlling the thermal effects, other discharge components such as reactive species concentrations and emission can vary with V_{p2p}. Next, we discuss how the reference maximum substrate temperature, $T_{\max}^{\mathrm{ref}}$, can be designed systematically in order to facilitate uniform thermal dose delivery.

5.2. Spatially uniform thermal dose delivery

As described in section 4, the dynamic optimization problem (4) enables designing the reference temperature $T_{\max}^{\mathrm{ref}}$ for the PI controller directly in terms of the desired thermal dose delivery objective specified in (5). Here, we consider offline and online solution of the optimization problem (4) for, respectively, open-loop and closed-loop dose delivery planning under the four translation trajectories shown in figure 5. For the translation trajectory of Case III, figure 7 shows the spatial thermal dose delivered at the end of the treatment time 5 min, the $T_{\max}$ profile, and the V_{p2p} profile for the cases of: (a) no feedback control and dose delivery planning, (b) the open-loop dose delivery planning strategy, and (c) the closed-loop dose delivery planning strategy. As seen in figure 7(a), $T_{\max}$ exhibits high variability and sensitivity to the APPJ translation when no feedback control is used for regulating $T_{\max}$. The inability to plan the dose delivery in this case, along with the variabilities in $T_{\max}$, leads to significant non-uniformity in the spatial dose delivery along the target region. For example, the thermal dose delivered at $x = -5$ mm is significantly lower than the desired thermal dose reference (i.e. $\mathrm{CEM}_{\mathrm{T}}^{\mathrm{ref}}(5, x) = 1$ min), whereas at $x = 5$ mm the delivered thermal dose is approximately twice the reference. Thus, the results suggest that the safety and effectiveness of dose delivery can be severely compromised in the case of no feedback control and dose delivery planning.

Figure 7(b) shows the results obtained using the open-loop dose delivery planning strategy, where the reference of the PI controller is determined by solving the optimization problem (4) once, offline. As expected, the PI controller can effectively track the offline-computed reference profile for the maximum substrate temperature, $T_{\max}^{\mathrm{ref}}$, while mitigating the variabilities that stem from the APPJ translation and possibly

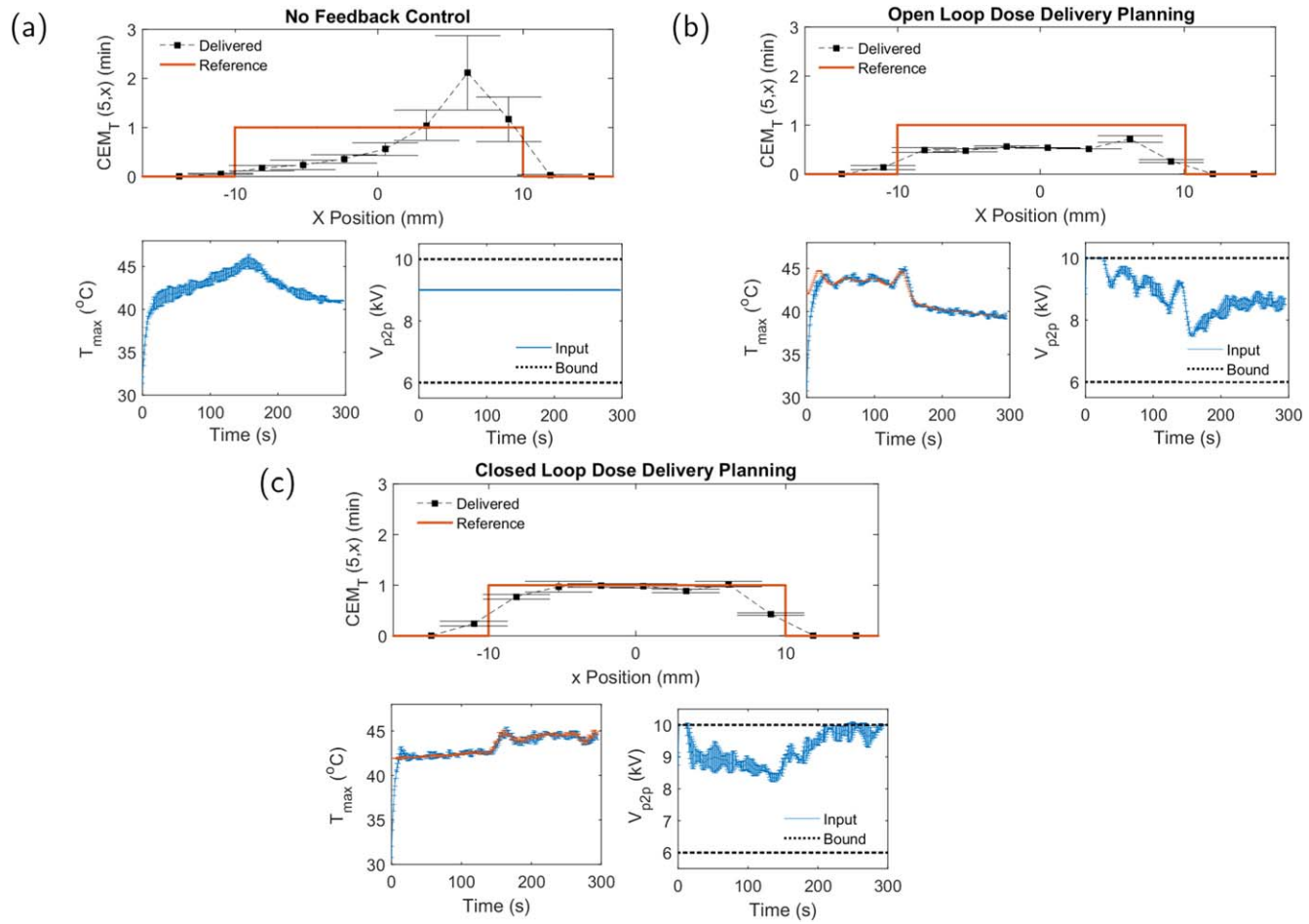

Figure 7. Delivered thermal dose $\mathrm{CEM_T}(5, x)$ along $x \in [-10, 10\ \mathrm{mm}]$, maximum substrate temperature $T_{\max}$, and applied peak-to-peak voltage V_{p2p} under the APPJ translation trajectory of Case III in figure 5 for: (a) no feedback control and dose delivery planning, (b) the open-loop dose delivery planning strategy, and (c) the closed-loop dose delivery planning strategy. The error bars show the standard deviation of variables based on three replicate runs.

other unknown sources of disturbances. Yet, even though a significantly more uniform thermal dose is achieved relative to the case of no feedback control, there is an offset between the delivered thermal dose and the reference dose. This can be attributed to the discrepancy between the planned dose and the actual thermal dose delivered due to the fact that the reference profile $T_{\max}^{\mathrm{ref}}$ is determined offline and thus it is blind to the actual state of dose delivery during the plasma treatment. On the other hand, the closed-loop dose delivery planning strategy mitigates this discrepancy via real-time solution of the optimization problem (4). In this case case, the actual thermal dose delivered to the substrate is inferred from temperature measurements every 6 s and is fed back to the supervisory controller (see figure 4). This allows online computation of the reference temperature $T_{\max}^{\mathrm{ref}}$ sent to the PI controller. Figure 7(c) suggests that the closed-loop dose delivery planning enables achieving a close to uniform thermal dose along the target region at the end of the treatment time, while maintaining high reproducibility and low variability in the dose delivery.

Next, we investigate the effect of the APPJ translation rate on the spatial thermal dose delivery. Figure 8 shows the delivered thermal dose using the open-loop and closed-loop dose delivery planning strategies under the APPJ translation rates of Cases I–IV given in table 1, which correspond to the four APPJ translation trajectories shown in figure 5. APPJ translation along the prespecified trajectories perturbs the substrate temperature dynamics, thus acting as a disturbance on the thermal dose delivery. Figure 8(a) suggests that neither the open-loop nor the closed-loop dose delivery planning strategy enables achieving spatially uniform thermal dose delivery in Case I. This can be attributed to the large, discrete steps of the APPJ translation, which prevent the substrate from being uniformly treated.[1] Figure 8 shows that a fairly uniform dose delivery can be achieved along the target region as the APPJ translation rate is increased in Cases II–IV. Higher translation rates result in smaller discrete translation steps, toward continuous APPJ translation in Case IV (see figure 5). This observation suggests there should exist a minimum translation rate below which uniform dose delivery is impractical.

[1] We note that similar nonuniformity in treatment is also observed in the case of discrete device translation strategies in radiotherapy applications [33].

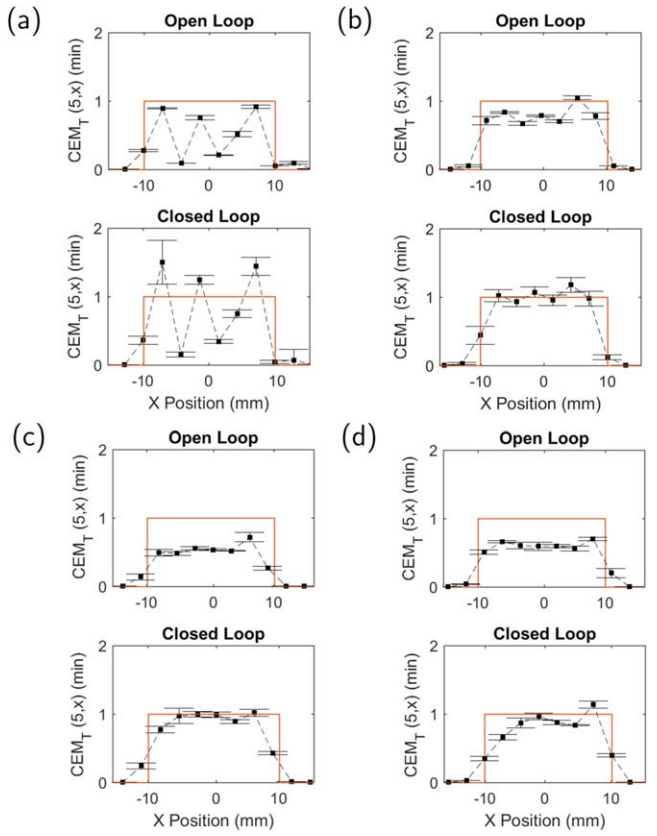

Figure 8. Delivered thermal dose $\mathrm{CEM_T}(5,\,x)$ along $x \in [-10,\,10\ \mathrm{mm}]$ using the open-loop and closed-loop dose delivery planning strategies under the APPJ translation rates of (a) Case I, (b) Case II, (c) Case III, and (d) Case IV. The red profiles depict the reference thermal dose $\mathrm{CEM}_{\mathrm{T}}^{\mathrm{ref}}(5,\,x)$. The error bars show the standard deviation of the delivered thermal dose based on three replicate runs.

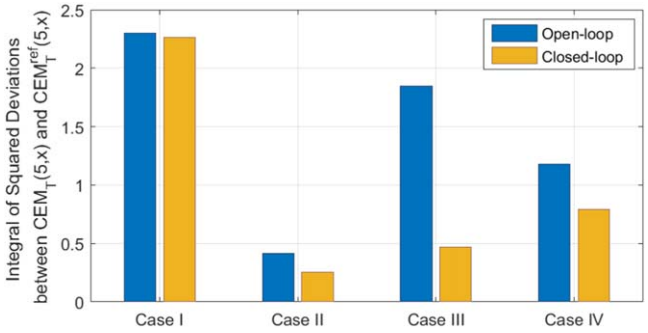

Figure 9. Performance comparison of the open-loop and closed-loop dose delivery planning strategies under the different APPJ translation rates. The dose delivery performance is quantified as the integral of squared deviations between the delivered, $\mathrm{CEM_T}(5,\,x)$, and reference, $\mathrm{CEM}_{\mathrm{T}}^{\mathrm{ref}}(5,\,x)$, thermal dose.

Furthermore, figure 8 shows that, irrespective of the APPJ translation rate, the open-loop dose delivery planning strategy leads to an offset in dose delivery with respect to the reference thermal dose. On the other hand, the closed-loop strategy enables realizing the reference thermal dose level of $\mathrm{CEM}_{\mathrm{T}}^{\mathrm{ref}}(5,\,x) = 1$ fairly uniformly along the target region. The performance comparison of the open-loop and closed-loop strategies under the different APPJ translation rates is summarized in figure 9, where the dose delivery performance is quantified as the integral of squared deviations between the delivered and reference thermal dose, i.e.

$$\int_{-10}^{10} \|\mathrm{CEM_T}(5,\,x)\mathrm{d}x - \mathrm{CEM}_{\mathrm{T}}^{\mathrm{ref}}(5,\,x)\|^2\,\mathrm{d}x.$$

Note that the expression above is in fact the first term in the objective function of the optimization problem in the supervisory controller (see (4*a*)). Figure 9 indicates that the closed-loop dose delivery planning strategy consistently outperforms the open-loop strategy under the four translation rates. However, as the translation rate increases from Case II to IV, the performance of the closed-loop dose delivery planning strategy slightly deteriorates. This can be attributed to the fact that a higher rate of the APPJ translation will perturb the spatial distribution of the delivered thermal dose more significantly.

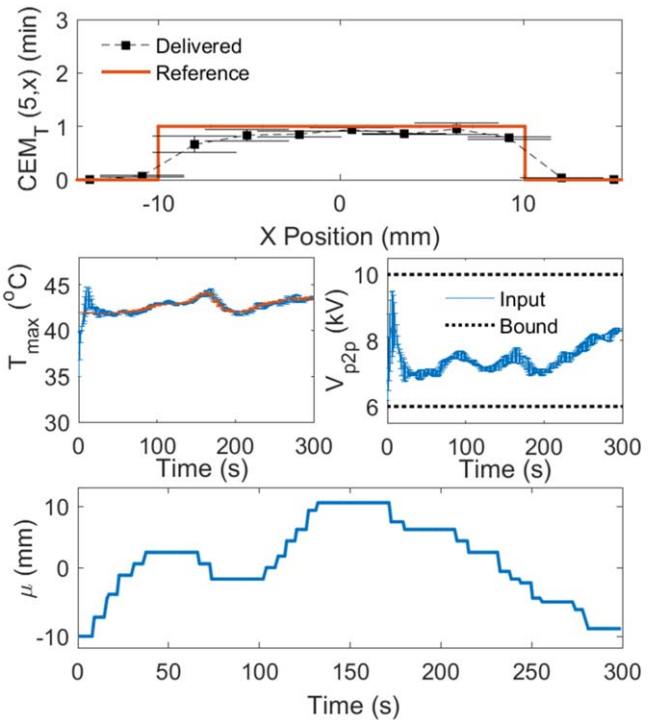

Figure 10. Delivered thermal dose $\mathrm{CEM_T}(5,\,x)$ along $x \in [-10,\,10\ \mathrm{mm}]$, maximum substrate temperature T_{max}, and applied peak-to-peak voltage V_{p2p} for the closed-loop dose delivery planning strategy under the offline-computed optimal APPJ translation trajectory μ. The error bars show the standard deviation of variables based on three replicate runs.

5.3. Thermal dose delivery under optimal APPJ translation trajectory

The dynamic optimization problem (4) can be modified to include the APPJ translation trajectory $\mu(t)$ as a decision variable, along with the reference temperature $T_{\mathrm{max}}^{\mathrm{ref}}$. Figure 10 shows the delivered thermal dose using the closed-loop dose delivery planning strategy when the optimal APPJ translation trajectory is computed offline. Interestingly, the optimal APPJ

trajectory has some resemblance to the translation trajectory of Case III (see figure 5) in that the APPJ is translated to the end of target region and back. In comparison with the thermal dose delivery under the trajectories of Cases II and III (see figure 5), the optimal translation trajectory results in slight improvement in the dose delivery.

6. Conclusion

This paper investigated the usefulness of advanced feedback control methods for real-time regulation of thermal dose delivery using a kHz-excited APPJ in helium. To this end, we proposed a hierarchical, feedback control strategy, which consists of a proportional-integral controller for fast disturbance rejection and a supervisory, optimization-based controller for online planning of the thermal dose delivery. Although this work focuses only on the thermal effects of plasma, the proposed strategy can be readily extended to include multiple plasma effects. As demonstrated in [20], optimization-based control strategies can accommodate multivariable dynamics. The key challenges in development of practical and comprehensive control strategies for APPJ remain in effective sensing and tractable modeling of complex plasma effects including chemistry. Particularly, models of plasma dose defined in terms of measurable plasma properties is an essential component for regulation of dose delivery.

The real-time control experiments demonstrated that the PI controller could significantly reduce the variability of the plasma operation. whereas the supervisory controller enabled achieving close-to-uniform dose delivery along the one-dimensional target region under different translation rates of the APPJ. In our future work, we will focus on development of effective real-time sensing and control strategies for uniform thermal dose delivery on two-dimensional surfaces with nonuniform electrical and thermal characteristics.

Acknowledgments

This work was supported in part by the U.S. Department of Energy, OFES Grant SC0001939, and in part by the Donors of the American Chemical Society Petroleum Research Fund under PRF 56627-DNI9.

Appendix. Tuning of the PI controller

The proportional-integral (PI) controller in the hierarchical, feedback control strategy of figure 4 is tuned using the internal model control (IMC) approach. An empirical model of the maximum substrate temperature T_{max} dynamics was first obtained via multiple-step test perturbation of the applied peak-to-peak voltage V_{p2p}, as shown in figure A1. It was observed that a first-order transfer function could adequately describe the T_{max} dynamics within the operating region of interest. The IMC tuning rules were then used to determine

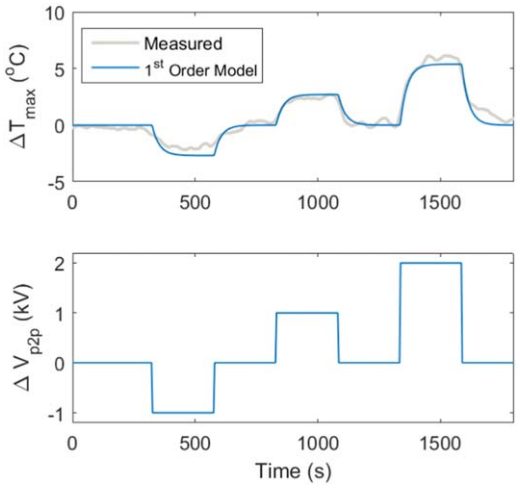

Figure A1. Multiple-step test perturbation of the applied peak-to-peak voltage V_{p2p} to characterize the dynamics of the maximum substrate temperature T_{max}. A first-order transfer function can adequately describe the T_{max} dynamics.

Table A1. Proportional gain (k_p) and integral-time constant (τ_I) of the PI controller.

k_p	τ_I
0.133 °C kV^{-1}	28.8 s

the two tuning parameters of the PI controller based on the transfer-function model of T_{max} dynamics [29]. The tuning parameters of the PI controller are given in table A1.

ORCID iDs

Dogan Gidon https://orcid.org/0000-0001-5832-4698
Ali Mesbah https://orcid.org/0000-0002-1700-0600

References

[1] Weltmann K-D, Kindel E, Brandenburg R, Meyer C, Bussiahn R, Wilke C and von Woedtke T 2009 Atmospheric pressure plasma jet for medical therapy: plasma parameters and risk estimation *Contrib. Plasma Phys.* **49** 631–40
[2] Shimizu T *et al* 2008 Characterization of microwave plasma torch for decontamination *Plasma Process. Polym.* **5** 577–82
[3] Metelmann H R, Seebauer C, Rutkowski R, Schuster M, Bekeschus S and Metelmann P 2018 Treating cancer with cold physical plasma: on the way to evidence-based medicine *Contrib. Plasma Phys.* **58** 1–5
[4] Isbary G, Zimmermann J L, Shimizu T, Li Y F, Morfill G E, Thomas H M, Steffes B, Heinlin J, Karrer S and Stolz W 2013 Non-thermal plasma—more than five years of clinical experience *Clin. Plasma Med.* **1** 19–23
[5] Podgorsak E 2006 *Radiation Oncology Physics: A Handbook for Teachers and Students* (Vienna: International Atomic Energy Agency)
[6] Laroussi M and Leipold F 2004 Evaluation of the roles of reactive species, heat, and UV radiation in the inactivation of

bacterial cells by air plasmas at atmospheric pressure *Int. J. Mass Spectrom.* **233** 81–6
[7] Lackmann J W, Schneider S, Edengeiser E, Jarzina F, Brinckmann S, Steinborn E, Havenith M, Benedikt J and Bandow J E 2013 Photons and particles emitted from cold atmospheric-pressure plasma inactivate bacteria and biomolecules independently and synergistically *J. R. Soc. Interface* **10** 20130591
[8] Sapareto S A and Dewey W C 1984 Thermal dose determination in cancer therapy *Int. J. Radiat. Oncol. Biol. Phys.* **10** 787–800
[9] Hildebrandt B, Wust P, Ahlers O, Dieing A, Sreenivasa G, Kerner T, Felix R and Riess H 2002 The cellular and molecular basis of hyperthermia *Crit. Rev. Oncol./ Hematology* **43** 33–56
[10] Kong M G, Kroesen G, Morfill G, Nosenko T, Shimizu T, van Dijk J and Zimmermann J L 2009 Plasma medicine: an introductory review *New J. Phys.* **11** 115012
[11] Lu X, Laroussi M and Puech V 2012 On atmospheric-pressure non-equilibrium plasma jets and plasma bullets *Plasma Sources Sci. Technol.* **21** 034005
[12] Gerling T, Nastuta A V, Bussiahn R, Kindel E and Weltmann K-D K-D 2012 Back and forth directed plasma bullets in a helium atmospheric pressure needle-to-plane discharge with oxygen admixtures *Plasma Sources Sci. Technol.* **21** 034012
[13] Walsh J L, Iza F, Janson N B, Law V J and Kong M G 2010 Three distinct modes in a cold atmospheric pressure plasma jet *J. Phys. D: Appl. Phys.* **43** 075201
[14] Liu J J and Kong M G 2011 Sub-60c atmospheric helium-water plasma jets: modes, electron heating and downstream reaction chemistry *J. Phys. D: Appl. Phys.* **44** 345203
[15] Gerber I, Mihaila I, Hein D, Nastuta A, Jijie R, Pohoata V and Topala I 2017 Time behavior of helium atmospheric pressure plasma jet electrical and optical parameters *Appl. Sci.* **7** 812
[16] Shin J and Raja L L 2007 Run-to-run variations, asymmetric pulses, and long time-scale transient phenomena in dielectric-barrier atmospheric pressure glow discharges *J. Phys. D: Appl. Phys.* **40** 3145–54
[17] Dünnbier M, Schmidt-Bleker A, Winter J, Wolfram M, Hippler R, Weltmann K-D and Reuter S 2013 Ambient air particle transport into the effluent of a cold atmospheric-pressure argon plasma jet investigated by molecular beam mass spectrometry *J. Phys. D: Appl. Phys.* **46** 435203
[18] Norberg S A, Johnsen E and Kushner M J 2015 Helium atmospheric pressure plasma jets touching dielectric and metal surfaces *J. Appl. Phys.* **118** 1–13
[19] Hao Z, Ji S, Liu H and Song Y 2014 Effect of the grounded electrode on cold ar atmospheric pressure plasma jet generated with a simple dbd configuration *IEEE Trans. Plasma Sci.* **42** 824–32
[20] Gidon D, Curtis B, Paulson J A, Graves D B and Mesbah A 2018 Model-based feedback control of a khz-excited atmospheric pressure plasma jet *IEEE Trans. Radiat. Plasma Med. Sci.* **2** 129–37
[21] Schmidt-Bleker A, Winter J, Bösel A, Reuter S and Weltmann K-D 2016 On the plasma chemistry of a cold atmospheric argon plasma jet with shielding gas device *Plasma Sources Sci. Technol.* **25** 015005
[22] Gidon D, Graves D B and Mesbah A 2016 Model predictive control of thermal effects of an atmospheric pressure plasma jet for biomedical applications *Proc. American Control Conf.* 4889–94
[23] Gidon D, Graves D B and Mesbah A 2017 Effective dose delivery in atmospheric pressure plasma jets for plasma medicine: A model predictive control approach *Plasma Sources Sci. Technol.* **26** 85005–19
[24] Dobrynin D *et al* 2011 Live pig skin tissue and wound toxicity of cold plasma treatment *Plasma Med.* **1** 93–108
[25] Roti J L 2008 Cellular responses to hyperthermia (40–46 degrees C): cell killing and molecular events *Int. J. Hyperth.* **24** 3–15
[26] Dewhirst M W, Viglianti B L, Lora-Michiels M, Hanson M and Hoopes P J 2003 Basic principles of thermal dosimetry and thermal thresholds for tissue damage from hyperthermia *Int. J. Hyperth.* **19** 267–94
[27] von Woedtke T, Metelmann H-R and Weltmann K-D 2014 Clinical plasma medicine: state and perspectives of *in vivo* application of cold atmospheric plasma *Contrib. Plasma Phys.* **54** 104–17
[28] Alaei P, Higgins P D, Weaver R and Nguyen N 2004 Comparison of dynamic and step-and-shoot intensity-modulated radiation therapy planning and delivery *Med. Dosim.* **29** 1–6
[29] Rivera D E, Morari M and Skogestad S 1986 Internal model control: PID controller design *Ind. Eng. Chem. Process. Des. Dev.* **25** 252–65
[30] Seaborg D E, Edgar T F, Mellinchamp D A and Doyle F J 2011 *Process Dynamics and Control* (New York: Wiley)
[31] Andersson J, Åkesson J and Diehl M 2012 CasADi: a symbolic package for automatic differentiation and optimal control *Recent Advances in Algorithmic Differentiation* (Berlin: Springer) pp 297–307
[32] Wächter A and Biegler L T 2006 On the implementation of an interior-point filter line-search algorithm for large-scale nonlinear programming *Math. Program.* **106** 25–57
[33] Ezzell G A and Chungbin S 2001 The overshoot phenomenon in step-and-shoot imrt delivery *J. Appl. Clin. Med. Phys.* **2** 138–48